Vietnam Journal of Science and Technology ***62*** *(3) (2024) 496-508*

doi:10.15625/2525-2518/20092

Study on fabrication and optical properties of monodisperse Ag-Au alloy nanostructure

Le The Tam[1], Nguyen Thi Ngoc Linh[2, *], Saonilan Thapphanya[2, 3], Dinh Thi Truong Giang[1]

[1]*Vinh University, 182 Le Duan, Vinh City, Nghe An Province, Viet Nam*

[2]*Thai Nguyen University of Sciences, Tan Thinh Ward, Thai Nguyen City, Thai Nguyen Province, Viet Nam*

[3]*Pharmaceutical Factory No. 2, Vientiane, Laos*

[*]Email: *linhntn@tnus.edu.vn*

Received: 6 February 2024; Accepted for publication: 25 April 2024

Abstract. This study addresses challenges in various fields by creating a new method for uniform, size- and composition-controlled Ag-Au alloy nanoparticles in organic solvents. Building on prior research, we demonstrate control over nanoparticle properties by varying complexing agents, surfactants, and reducing agents. Optimal conditions using surfactant SOA and reducing agent TBAB yielded small, monodisperse Ag nanoparticles ideal for alloying with Au. The reaction time significantly impacts final morphology and surface plasmon resonance (SPR) properties of the resultant Ag-Au alloy nanoparticles. Interestingly, Au nanoparticles formed under identical conditions shared a similar size with 60-minute Ag-Au alloys, evidenced by a single SPR peak at 520 nm. This control over Ag-Au nanoalloy composition and size opens doors for promising applications.

Keywords: Nanostructure, Ag-Au alloy, reduction in organic solvents, monodisperse, optical properties.

Classification numbers: 2.2.1, 2.4.3.

1. INTRODUCTION

Noble metal nanoparticles (Ag, Au) and Au-Ag nanoalloys have garnered significant attention recently due to their intriguing catalytic, electronic, and optical properties [1 - 3]. Gold nanoparticles (Au NPs) and Ag-Au nanoalloys exhibit exceptional promise in various biomedical applications, including diagnostics, sensors, and biolabelling treatmenttechniques, and in vitro and in vivo studies [4 - 6]. Furthermore, bimetallic nanoparticles like Ag-Au hold particular interest in catalysis, often demonstrating superior catalytic efficiency compared to their monometallic counterparts [7]. This report delves into novel synthesis methods, size and structural characteristics, and surface plasmon resonance properties of Ag-Au bimetallic nanoparticles. Various synthesis techniques exist for producing spherical Ag-Au bimetallic nanoparticles, utilizing aqueous media, and organic solvents [8, 9]. Beyond the well-studied spherical morphology, bimetallic Ag-Au nanoparticles (NPs) have also been synthesized in

diverse shapes, such as triangular, square, rhombic, pentagonal, and octahedral [9]. The specific structure of these nano-sized particles is highly dependent on fabrication conditions, including the nucleation process (dictating the size and number of nuclei formed), reduction time of precursor ions, temperature, solvent choice, and the redox potentials of the two metals involved. Fundamentally, bimetallic NPs can adopt two main structural configurations: alloyed and core-shell. Typical Ag-Au alloy NPs are prepared by the simultaneous reduction of gold(III) and silver(I) ions using reducing agents like citrate, hydrazine hydrate or sodium borohydride [10 - 12]. In contrast, core-shell NPs involve the reduction of "shell" metal ions onto the pre-formed "core" nanoparticle surface. Various techniques have been reported in the literature for the selective removal of unwanted shell ions from the core particle surface. Chemical reduction techniques, including those utilizing citrate [13], ascorbic acid [14], borohydride and even natural Neem leaf extract [15], represent the most prevalent methods for synthesizing Ag-Au nanoparticles. Non-chemical approaches, such as UV irradiation, laser heating, and even microwave techniques, have also been explored [16, 17]. While many fabrication methods have been investigated and numerous research groups have presented results on the preparation and characterization of Ag-Au alloy and core-shell nanoparticles, detailed information regarding the fabricated alloy nanoparticles' size, structure, and morphology remains somewhat scarce [18]. Despite significant advancements in nanoparticle synthesis, the production of bimetallic nanoparticles, particularly alloyed structures, has seen limited progress in recent years. This stagnation is attributed to the inherent challenge of phase separation at the atomic level, often resulting in the formation of core-shell structures rather than true alloys. Consequently, achieving precise control over bimetallic nanoparticles' size and composition remains a significant hurdle. Firstly, manipulating synthesis parameters to adjust the size of bimetallic nanoparticles proves considerably more complex than single-component nanoparticles. Secondly, most existing methods require the ability to decouple size and composition control, hindering the production of nanoparticles with identical compositions yet varying sizes or vice versa. Furthermore, the tendency of Ag^+ ions to form halide precipitates during synthesis processes involving halogen-containing metal salt precursors (e.g., $HAuCl_4$) presents an additional challenge. The precipitation of AgCl affects the morphology of the formed alloy nanoparticles and complicates the control of their overall composition.

As previously mentioned, both monometallic and bimetallic noble metal nanoparticles exhibit unique optical properties from surface plasmon resonance (SPR). Interestingly, the specific expression of SPR differs between nanoalloys and core-shell structures, particularly within the visible range of the electromagnetic spectrum. Nanoalloys exhibit a single, characteristic plasmon band in the visible region, reflecting their precise composition. Conversely, core-shell nanoparticles showcase two distinct plasmon bands [18]. However, if the core-shell structure features an exceptionally thin shell (approximately 3 - 4 nm), only the plasmon band characteristic of the shell metal will be apparent in the spectrum [16]. This study tackled the challenge of controlling size and composition in Ag-Au alloy nanoparticles. We investigated how complexing agents, surfactants, reducing agents, and reaction time influence the formation of Ag nanoparticles and the resulting Ag-Au alloys. To characterize the synthesized nanoparticles, we employed transmission electron microscopy (TEM) for size and shape analysis, UV-Vis spectroscopy for studying their plasmonic properties, and energy-dispersive X-ray spectroscopy (EDX) to determine their elemental composition.

2. EXPERIMENTAL

2.1. Chemicals

All chemicals employed in the experiments were procured from Sigma-Aldrich (Singapore). These included gold(III) chloride trihydrate ($HAuCl_4.3H_2O$), silver nitrate ($AgNO_3$), oleylamine (OLA), sodium oleate (SOA), tert-butylamine-borane (TBAB), 1-octadecanol (OCD-ol), 1-octadecene (ODE), absolute ethanol (C_2H_5OH), and n-hexane (C_6H_{14}). All chemicals were utilized as received without any further purification.

2.2. Synthesis of Ag NPs

The synthesis of Ag and Ag-Au alloy NPs in this study was illustrated in Scheme 1. First, Ag NPs were fabricated by reduction method in an organic solvent. 6 mmol of $AgNO_3$ and 6 - 20 mmol (within the studied range) of sodium oleate (SOA) were added to a three-necked flask containing 20 mL of ODE. The mixture was stirred at room temperature under a continuous N_2 gas flow until a homogeneous solution was achieved. A reducing agent solution was prepared by mixing 0.5 - 2.5 mmol of tert-butylamine-borane (TBAB), 1 mL of oleylamine (OLA), and 1 mL of 1-octadecene (ODE) at room temperature until homogeneous. This reducing agent solution was then slowly added to the solution in the flask. The combined reaction mixture was stirred at room temperature for 60 minutes under continuous N_2 gas flow.

Following synthesis, Ag nanoparticles were repeatedly washed with ethanol and n-hexane to remove impurities. Centrifugation at 12,000 rpm for 10 minutes was then employed to collect Ag nanoparticles. Finally, the collected nanoparticles were dispersed in an n-hexane solvent for preservation and subsequent characterization.

2.3. Synthesis of Ag-Au alloy NPs

Ag-Au alloy nanoparticles were synthesized via the substitution method using previously fabricated Ag nanoparticles (Subsection 2.2) and $HAuCl_4.3H_2O$ precursor. In a three-neck flask containing 30 mL of 1-octadecene (ODE), 100 mg of Ag nanoparticles were added. Next, 50 mg of $HAuCl_4.3H_2O$ and 6 mL of oleylamine (OLA) were introduced, and the mixture was stirred at room temperature for 30 minutes. Subsequently, 0.3 g of 1-octadecanol (OCD-ol) dispersed in 10 mL of ODE was slowly added dropwise to the flask.

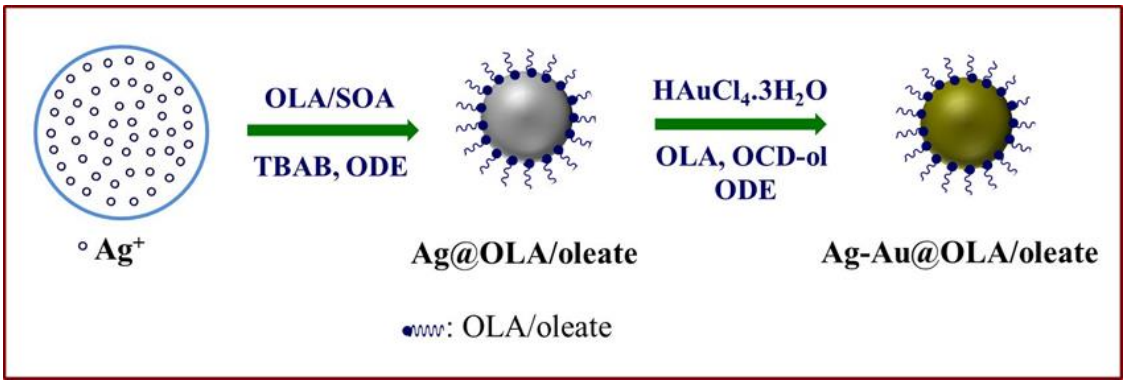

Scheme 1. Schematic illustration of the formation process of Ag/Au alloy NPs.

The reaction mixture was then stirred at 80 °C for 30 minutes. Afterwards, the temperature was increased to 180 °C and maintained under reflux for 30 - 120 minutes. Throughout the synthesis, a continuous flow of nitrogen gas was provided. Following the same washing procedure as described for Ag nanoparticles in Subsection 2.2, the product was repeatedly washed with ethanol and n-hexane to remove impurities. To selectively remove the AgCl byproduct formed during the synthesis, an excess amount of saturated ammonia solution was added to the material and subjected to ultrasonication for 10 minutes. This treatment facilitated the dissolution of AgCl. Subsequently, the product was centrifuged and thoroughly rinsed with distilled water to eliminate residual $[Ag(NH_3)_2]Cl$ and ammonia. As a control experiment, Au nanoparticles were synthesized using the same method but omitting the introduction of Ag seeds during the fabrication process.

2.4. Material characterization

The material's morphology was investigated using transmission electron microscopy (TEM) on a JEM JEOL-1010 (Japan) instrument operated at an acceleration voltage of 80 kV. The Ultraviolet-visible (UV-Vis) molecular absorption spectrum of the material was acquired with a Jasco V-670 spectrometer (Japan). Energy dispersive X-ray spectroscopy (EDX) analysis on a Jeol JSM-6510LV instrument was performed to determine the chemical composition of the material.

3. RESULTS AND DISCUSSION

3.1. Influence of reactants on the morphology and optical properties of Ag NPs

3.1.1. Morphology of Ag NPs

During the Ag nanomaterial synthesis process, sodium oleate (SOA) plays a dual role: acting both as an intermediate complexing agent for Ag^+ ions and as a surfactant to minimize nanoparticle aggregation [4, 19]. To elucidate the impact of SOA on the morphology of Ag nanomaterials, its concentration was varied from 6 to 20 mmol in the experiments. The shape and size of the resulting Ag nanoparticles were subsequently analyzed using transmission electron microscopy (TEM), as depicted in Figure 1.

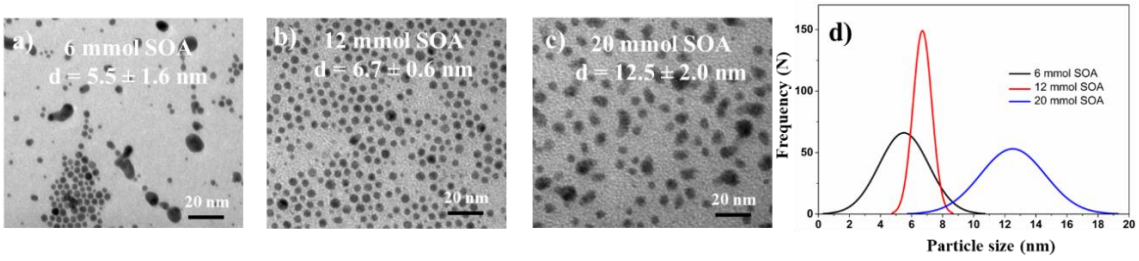

Figure 1. Typical TEM images (scale bar: 20 nm) of Ag NPs at different concentration surfaces (a-c), and corresponding size distribution histograms (d).

Figure 1 presents transmission electron microscopy (TEM) images and size distribution charts of Ag nanoparticles synthesized using 1.5 mmol of the reducing agent TBAB and varying amounts of SOA (6, 12, and 20 mmol). The results demonstrate a clear influence of SOA concentration on the nanoparticles' morphology and size. With the lowest SOA concentration (6

mmol), the TEM image (Figure 1a) reveals nearly spherical, uneven particles with an average diameter of 5.5 ± 1.6 nm. Notably, the error in this case is relatively large, reaching approximately 29 %, indicating a lack of monodispersity. Doubling the SOA concentration (to 12 mmol) leads to the formation of spherical, uniform, and monodisperse Ag nanoparticles with an average diameter of 6.7 ± 0.6 nm (Figure 1b). The significantly smaller error (around 9 %) suggests improved size control. Increasing the SOA concentration to 20 mmol (representing a 3.3-fold increase) produced uneven Ag nanoparticles (Figure 1c). Alongside spherical particles, the presence of near-rod-shaped nanoparticles was observed. Additionally, the average size increased to 12.5 ± 2.0 nm, with a particle size error of 16 %, indicating a loss of monodispersity compared to the 12 mmol sample. These observations demonstrate the significant impact of SOA concentration on both particle size and shape. As the SOA concentration increases, a trend of increasing particle size and shape transformation from spherical to near-rod-shaped becomes evident. This confirms the crucial role of SOA in regulating the size, shape, and uniformity of synthesized Ag nanomaterials.

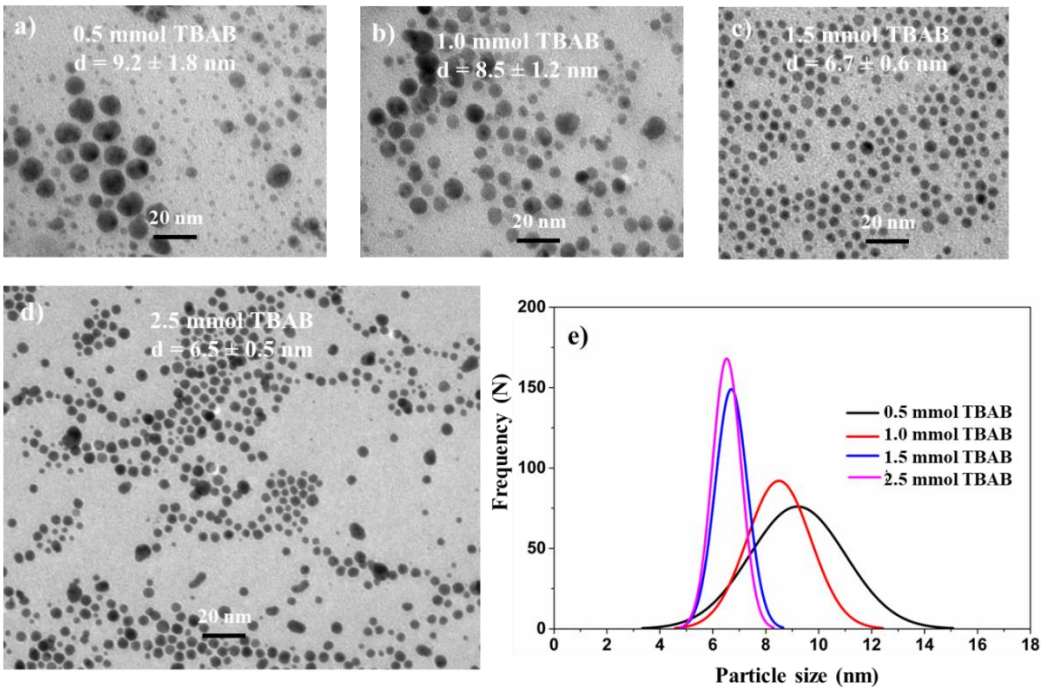

Figure 2. TEM images (a-d) and particle size distribution (e) of the nano Ag fabricated with different quantities of the TBAB reductant.

Further experiments explored the influence of the TBAB-reducing agent on the development and size of Ag nanoparticles. Figure 2 presents TEM images of samples synthesized with varying TBAB amounts (0.5, 1.0, 1.5, and 2.5 mmol) while maintaining a constant SOA concentration of 12 mmol. All other synthesis parameters remained unchanged. The results demonstrate a clear particle size and uniformity dependence on the TBAB concentration. Using 0.5 mmol TBAB yielded large, unequally sized particles with an average diameter of 9.2 ± 1.8 nm and a relatively high size error of 20 % (Figure 2a), indicating poor monodispersity and increasing the TBAB concentration to 1.0 mmol led to smaller and more uniform nanoparticles with an average diameter of 8.5 ± 1.2 nm and a significantly reduced size error of 14 % (Figure 2b). Notably, employing 1.5 mmol TBAB resulted in the smallest and

most uniform nanoparticles, exhibiting an average diameter of 6.7 ± 0.6 nm and a minimal size error of approximately 9 %. This suggests optimal control over size and uniformity at this particular TBAB concentration. Employing the highest TBAB concentration (2.5 mmol) resulted in Ag nanoparticles of comparable size (6.5 ± 0.6 nm) to the 1.5 mmol TBAB sample but with decreased uniformity (increased size error of 9.2 %, Figure 2d). These observations highlight the significant impact of TBAB concentration on particle size and uniformity. The larger and less uniform particles observed with lower TBAB concentrations are likely due to a reduced number of initial Ag crystal nuclei formed in the solution compared to higher decreasing agent amounts. At higher TBAB concentrations, the size limit for individual nanoparticles is reached more quickly, forming larger particles. Furthermore, established theories on crystal nucleus growth under low monomer concentrations and slow precursor reaction rates during synthesis posit the occurrence of Ostwald ripening. This phenomenon could also contribute to the broader size distribution observed in samples with lower TBAB contents, as documented in [20, 21].

Based on the TEM analysis, a combination of 12 mmol of SOA and 1.5 mmol of TBAB appears to be optimal for synthesizing Ag nanomaterials with desired characteristics, including small particle size and high uniformity. This finding highlights the critical role of adjusting these parameters during fabrication to achieve the targeted properties for Ag nanomaterials.

3.1.1. Optical properties of Ag NPs

The influence of reaction conditions on the optical properties of Ag nanomaterials was investigated using UV-Vis molecular absorption spectroscopy, with the results summarized in Table 1. As the concentration of the SOA surfactant increased from 6 to 20 mmol, a corresponding shift in the surface plasmon resonance (SPR) peak position was observed, ranging from 398 to 403 nm. This observed red shift can be attributed to the increasing average size of the Ag nanoparticles with higher SOA concentrations. Conversely, increasing the concentration of the TBAB reducing agent led to a blue shift in the SPR peak position, from 402 to 399 nm, due to the resulting decrease in nanoparticle size. Under the reaction conditions explored, where the size of the synthesized Ag nanoparticles ranged from 5.5 to 12.5 nm, the SPR peak position varied between 398 and 403 nm (Table 1).

Table 1. The influence of reaction conditions on optical properties of the nano Ag.

$AgNO_3$ (mmol)	**SOA (mmol)**	**TBAB (mmol)**	**Reaction temperature (^oC)**	**Reaction time (min)**	**Average particle size (nm)**	**SPR position (nm)**
6	6	1.5	30	60	5.5 ± 1.6	398
	12				6.7 ± 0.6	399
	20				12.5 ± 2.0	403
6	12	0.5	30	60	9.2 ± 1.8	402
		1.0			8.5 ± 1.2	401
		1.5			6.7 ± 0.6	399
		2.5			6.5 ± 0.5	399

Figure 3 depicts the UV-Vis spectra of representative Ag nanoparticle samples categorized by their average particle sizes: 6.7 ± 0.6 nm (Ag-6.7), 8.5 ± 1.2 nm (Ag-8.5), and 9.2 ± 1.8 nm (Ag-9.2). As expected, all samples exhibit a surface plasmon resonance (SPR) band characteristic of elemental Ag. Notably, the SPR peak positions directly correlate with particle

size: 399 nm for Ag-6.7, 401 nm for Ag-8.5, and 402 nm for Ag-9.2. This red shift in peak position with increasing particle size is attributed to the influence of size and shape on the SPR phenomenon. Our findings align with previous reports describing Ag nanoparticle synthesis in organic solvents by Lakshminarayana Polavarapu's group [22] and in water solvents by Meng Chen's group [23].

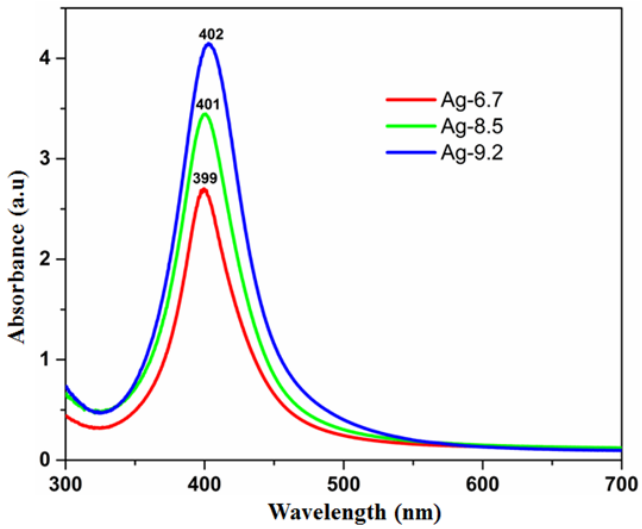

Figure 3. UV-Vis spectra of some nano Ag with different sizes.

3.2. Ag-Au alloy structure

3.2.1. Morphology of Ag-Au alloy NPs

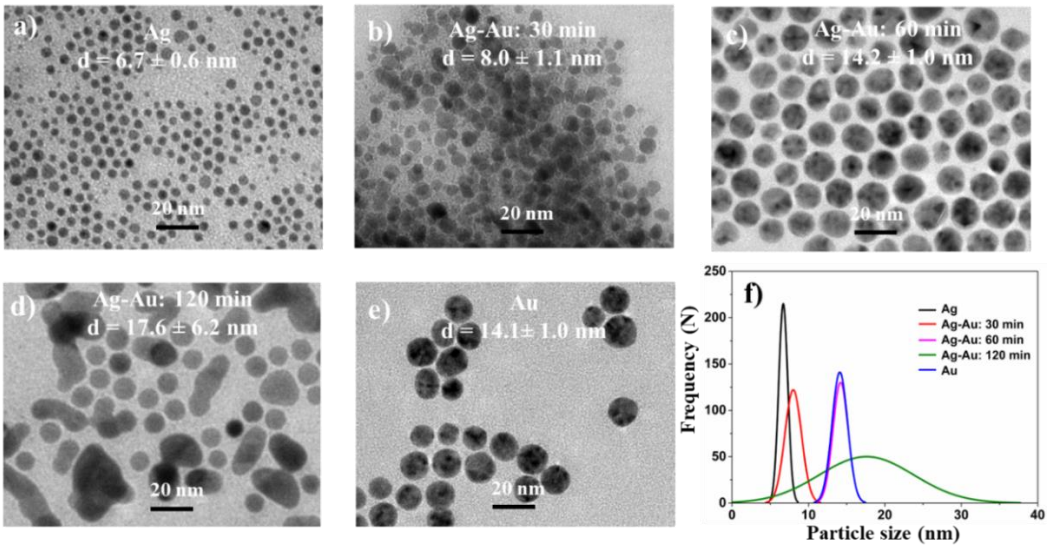

Figure 4. TEM images (a-e) and particle size distribution (f) of the nano Ag, Ag-Au alloy and Au fabricated at different times, from 30 to 120 min.

This study explores the fabrication of Ag-Au alloy nanoparticles through a substitution reaction between Ag nanoparticles and $HAuCl_4.3H_2O$ in an ODE solvent. As starting material, we employed Ag nanoparticles with a well-defined size of 6.7 ± 0.6 nm (Figure 4a). The influence of reaction time on the morphology of the resulting Ag-Au nanoalloys was investigated using transmission electron microscopy (TEM). Detailed morphological information is presented in Figure 4.

The reaction time significantly influenced the morphology and uniformity of Ag-Au alloy nanoparticles. Following a 30-minute reaction, TEM images (Figure 4a) revealed spherical nanoparticles with indistinct grain boundaries and an average size of 8.0 ± 1.1 nm, indicating moderate size dispersity (error ~14 %). Extending the reaction time to 60 minutes resulted in forming predominantly spherical and relatively uniform Ag-Au alloy nanoparticles (Figure 4b). Notably, the average particle size increased to 14.2 ± 1.0 nm with a lower error of ~7 %. However, increasing the reaction time to 120 minutes led to unevenly shaped nanoparticles alongside spherical ones, accompanied by particle aggregation (Figure 4c). This resulted in a significant increase in average size (17.6 ± 6.2 nm) and a substantial size error of 35.2 %, highlighting the loss of uniformity. These observations demonstrate a clear trend of increasing particle size and decreasing uniformity with longer reaction times. Prolonging the reaction time enhances the movement of particles, leading to an increase in their surface energy. This drives the nanoparticles to coalesce, minimizing their total surface energy through aggregation. Consequently, larger particles are formed within the reaction system, a phenomenon known as Ostwald ripening [24]. As a control experiment, Au nanoparticles synthesized under identical conditions exhibited an average diameter of 14.1 ± 1.0 nm (Figure 4e). Notably, this size corresponds to the Ag-Au alloy nanoparticles obtained after 60 minutes of reaction, highlighting the influence of extended reaction time on particle growth in both pure Au and Ag-Au systems.

The formation of Ag-Au alloy nanoparticles in this study can be described as follows: Since the standard reduction of the $AuCl_4^-$/Au pair (1.0 V) is higher than that of Ag^+/Ag (0.80 V), Ag nanoparticles are oxidized by $AuCl_4^-$ to Ag^+ according to the following substitution reaction [25]:

$$3Ag + AuCl_4^- \rightarrow Au + Cl^- + 3AgCl\downarrow \quad (1)$$

The oxidation of Ag nanoparticles by $AuCl_4^-$ generates Au atoms. Under suitable reaction conditions, these Au atoms deposit onto the Ag nanoparticle surface, alloying with the unreacted Ag to form homogeneous Ag-Au alloy nanoparticles [42]. Subsequently, the AgCl byproduct is removed using a concentrated NH_3 solution, following the washing procedure described in Subsection 2.3.

$$AgCl + 2NH_3 \rightarrow [Ag(NH_3)_2]Cl. \quad (2)$$

3.2.2. Optical properties of Ag-Au alloy NPs

Investigation of the optical properties of the single metal NPs (Ag, Au) and the alloy was conducted using UV-Vis molecular adsorption spectroscopy. Figures 5a and b represent our results.

The characteristic colors exhibited by Ag and Au nanoparticle solutions were found to be dependent on their size and shape. The Ag nanoparticle solution appeared yellow, corresponding to its maximum absorbance at 399 nm. Conversely, the Au nanoparticle solution displayed a purple color, coinciding with its absorption peak at 520 nm. As evident in Figure 5a, the color of the Ag-Au alloy nanosystem progressively transitions from yellow to purple with increasing

reaction time. Inspection of the UV-Vis spectrum in Figure 5b reveals that the absorption peaks of Ag-Au alloy nanoparticles span a wider range within the UV-Vis spectrum as the sample fabrication time increases. Notably, the sample prepared at 30 minutes exhibits two distinct surface plasmon resonance peaks at 409 and 477 nm. This observation suggests the formation of non-homogeneous alloy nanoparticles, where some Ag nanoparticles (seeds) possess a higher concentration of deposited Au atoms than others. This heterogeneity is further supported by the uneven distribution of nanoparticles observed in the TEM image (Figure 4b). Extending the reaction time to 60 minutes resulted in an Ag-Au nano sample with an absorption peak at 520 nm, identical to the peak of free Au nanoparticles of comparable size. Notably, the 120-minute sample exhibited a slight red shift of the peak position (523 nm) accompanied by a broader peak compared to the 60-minute sample. This observation aligns with the increase in Ag-Au nanoparticle size observed at longer reaction times (Table 2), potentially leading to particle aggregation and the formation of larger structures (Figure 4d). These findings highlight the strong dependence of surface plasmon resonance (SPR) absorption position and shape on particle size and shape, corroborating the predictions of Mie theory [26]. Furthermore, the absence of two distinct SPR peaks, characteristic of physically mixed Ag and Au nanoparticles [27], confirms the formation of true Ag-Au alloys rather than simple mixtures.

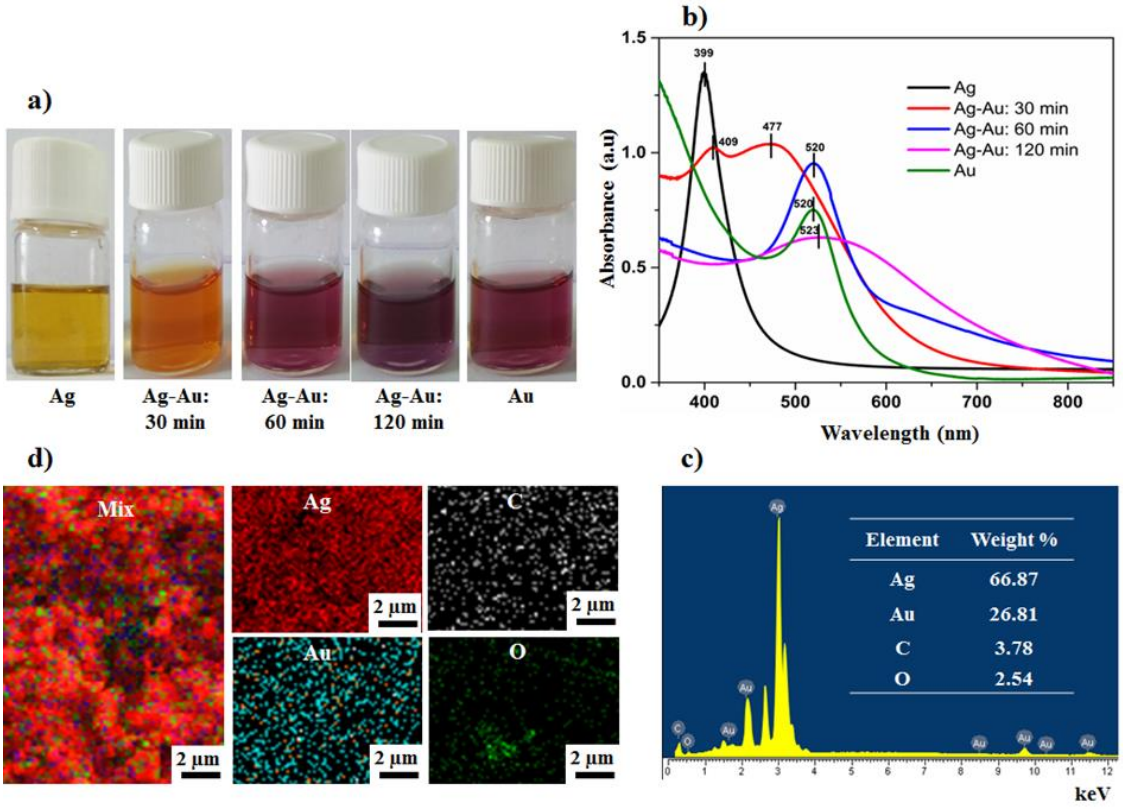

Figure 5. Images of solutions (a) and spectra (b) of the nano-Ag, Au, and alloy fabricated at different reaction times from 30 to 120 minutes, EDX spectra and mass percentage of elements (c), EDX elemental mapping (d) of Ag-Au alloy NPs synthesized at 60 minutes.

Energy-dispersive X-ray spectroscopy (EDX) analysis of the Ag-Au alloy nano sample fabricated at 60 minutes (Figure 5c) revealed intense peaks characteristic of both Ag and Au elements. The quantitative analysis indicated atomic percentages of 66.87 % Ag and 26.81 %

Au, corresponding to a ratio of ~ 2.5:1. Minor peaks for C and O elements with respective atomic percentages of 3.78 % and 2.54 % were also observed. This presence is attributed to the oleate surfactant coating the nanoparticle surface, as documented in previous studies [28]. Furthermore, elemental mapping (Figure 5d) confirmed the homogeneous distribution of elements within the Ag-Au alloy nanoparticles.

Table 2. Influence of synthesis conditions on the optical properties of the alloy Ag-Au NPs.

Nanomaterial	**Reaction time (min)**	**Average particle size (nm)**	**SPR position (nm)**
Ag	60	6.7 ± 0.6	399
Ag-Au	30	8.0 ± 1.1	409 and 477
	60	14.2 ± 1.0	520
	120	17.6 ± 6.2	523
Au	60	14.0 ± 0.9	520

4. CONCLUSIONS

We fabricated monodisperse, spherical Ag and Ag-Au alloy nanoparticles in organic solvents. By optimizing conditions, we controlled nanoparticle size and composition. A specific SOA surfactant and TBAB reductant combo yielded ideal, small Ag nanoparticles for alloying. The final Ag-Au alloy morphology and uniformity were controlled by the reaction time. Interestingly, pure Au nanoparticles matched the size of 60-minute Ag-Au alloys (single SPR peak at 520 nm). Characterization of the fabricated nanoparticles revealed a size range of 5.5 - 12.5 nm for Ag nanoparticles with a corresponding SPR position of 398 - 403 nm. Ag-Au alloy nanoparticles exhibited a spherical shape with average grain sizes between 8.0 and 17.6 nm, and a wider SPR absorption range (477 - 523 nm). Further analysis of the 60-minute Ag-Au sample revealed an Ag:Au ratio of 2.5:1 at the atomic level. This precise size and composition control opens doors for applying these Ag-Au alloys in various fields.

Acknowledgment. This research was supported by the Project of the TNU-University of Sciences in Viet Nam under grant number CS2021-TN06-17.

CRediT authorship contribution statement. Le The Tam, Nguyen Thi Ngoc Linh, Saonilan Thapphanya, Dinh Thi Truong Giang: Synthesis, Analysis, and Assessment of morphology and structure of materials. Nguyen Thi Ngoc Linh: Supervision, Writing - original draft. Le The Tam: Writing - review & Editing. All authors read and approved the final manuscript.

Declaration of competing interest. There are no conflicts to declare.

REFERENCES

1. Qiao X., Yu K., Xu J., Cai Y., Li Y., Cao H., Lü J. - Engineered nanoscale schwertmannites as Fenton–like catalysts for highly efficient degradation of nitrophenols, Appl. Surf. Sci. **548** (15) (2021) 149248. https://doi.org/10.1016/j.apsusc.2021.149248.
2. Sareen S., Mutreja V., Pal B., Singh S. - Synthesis of bimetallic Au-Ag alloyed mesocomposites and their catalytic activity for the reduction of nitroaromatics, Appl. Surf. Sci. **435** (30) (2018) 552-562. https://doi.org/10.1016/j.apsusc.2017.11.152.

3. Heinz M., Srabionyan V. V., Avakyan L. A., Bugaev A. L., Skidanenko A. V., Kaptelinin S. Y., Bugaev L. A. - Formation of bimetallic gold-silver nanoparticles in glass by UV laser irradiation, J. Alloys Compd. **767** (30) (2018) 1253-1263. https://doi.org/10.1016/j.jallcom.2018.07.183.
4. Nguyen T. N. L., Le T. T., Nguyen H. D., Nguyen D. V., Phan T.H. T., Bui M. Q., Cao T. A., Nguyen T. S., Le T. L. - Synthesis and properties of Ag-Au alloy nanoparticles with controlled composition for computed tomography imaging applications, ChemNanoMat **10** (5) (2024) e202300619. https://doi.org/10.1002/cnma.202300619.
5. Liao W., Liu K., Chen Y., Hu J., Gan Y. - Au-Ag bimetallic nanoparticles decorated silicon nanowires with fixed and dynamic hot spots for ultrasensitive 3D SERS sensing, J. Alloys Compd. **868** (2021) 159136. https://doi.org/10.1016/j.jallcom.2021.159136.
6. Jiao A., Dong X., Zhang H., Xu L., Tian Y., Liu X., Chen M. - Construction of pure worm-like AuAg nanochains for ultrasensitive SERS detection of pesticide residues on apple surfaces, Spectrochimica Acta Part A: Mol. Biomol. Spectrosc. **209** (2019) 241-247. https://doi.org/10.1016/j.saa.2018.10.051.
7. Arora N., Mehta A., Mishra A., Basu S. - 4-Nitrophenol reduction catalysed by Au-Ag bimetallic nanoparticles supported on LDH: Homogeneous vs. heterogeneous catalysis, Appl. Clay Sci. **151** (2018) 1-9. https://doi.org/10.1016/j.clay.2017.10.015.
8. Mott D., Thuy N. T. B., Aoki Y., Maenosono S. - Aqueous synthesis and characterization of Ag and Ag-Au nanoparticles: addressing challenges in size, monodispersity and structure, Philosophical Transactions of the Royal Society A: Mathematical, Physical and Engineering Sciences **368** (1927) (2010) 4275-292. https://doi.org/10.1098/rsta.2010.0120.
9. Wu Y., Jiang P., Jiang M., Wang T., Guo C., Xie S.., Wang Z. - The shape evolution of gold seeds and gold@silver core-shell nanostructures, Nanotechnology **20** (30) (2009) 305602. https://doi.org/10.1088/0957-4484/20/30/305602.
10. Devarajan S., Vimalan B., Sampath S. - Phase transfer of Au-Ag alloy nanoparticles from aqueous medium to an organic solvent: Effect of aging of surfactant on the formation of Ag-rich alloy compositions, J. Colloid Interface Sci. **278** (1) (2004) 126-132. https://doi.org/10.1016/j.jcis.2004.05.038.
11. Pal A., Shah, S., Devi S. - Synthesis of Au, Ag and Au-Ag alloy nanoparticles in aqueous polymer solution, Colloids and Surfaces A: Physicochem. Eng. Asp. **302** (1-3) (2007) 51-57. https://doi.org/10.1016/j.colsurfa.2007.01.054.
12. Wilcoxon J. - Optical absorption properties of dispersed gold and silver alloy nanoparticles, J. Phys. Chem. B **113** (9) (2009) 2647-2656. https://doi.org/10.1021/jp806930t.
13. Kim Y., Johnson R. C., Li J., Hupp J. T., Schatz G. C. - Synthesis, linear extinction, and preliminary resonant hyper-Rayleigh scattering studies of gold-core/silver-shell nanoparticles: Comparisons of theory and experiment, Chem. Phys. Lett. **352** (5-6) (2002) 421-428. https://doi.org/10.1016/S0009-2614(01)01506-8.
14. Ma Yanyun., Li W., Cho E. C., Li Z., Yu T., Zeng J., Xie Z., Xia Younan. - Au@Ag core-shell nanocubes with finely tuned and well-controlled sizes, shell thicknesses, and optical properties, ACS Nano **4** (11) (2010) 6725-6734. https://doi.org/10.1021/nn102237c.
15. Shankar S. S., Rai A., Ahmad A., Sastry M. - Rapid synthesis of Au, Ag, and bimetallic Au core-Ag shell nanoparticles using Neem (Azadirachta indica) leaf broth, J. Colloid

Interface Sci. **275** (2004) 496-502. doi: https://doi.org/10.1016/j.jcis.2004.03.003.

16. Mallik K., Mandal M., Pradhan N., Pal T. - Seed mediated formation of bimetallic nanoparticles by uv irradiation: A photochemical approach for the preparation of "Core-Shell" type structures, Nano Lett. **1** (6) (2001) 319-322. https://doi.org/10.1021/nl0100264.
17. Peng Z., Spliethoff B., Tesche B., Walther T., Kleinermanns K. - Laser-assisted synthesis of Au - Ag alloy nanoparticles in solution, J. Phys. Chem. B **110** (6) (2006) 2549-2554. https://doi.org/10.1021/jp056677w.
18. Chen H. M., Liu R. S., Jang L. Y., Lee J. F., Hu S. F. - Characterization of core-shell type and alloy Ag/Au bimetallic clusters by using extended X-ray absorption fine structure spectroscopy, Chem. Phys. Lett. **421** (1-3) (2006) 118-123. https://doi.org/10.1016/j.cplett.2006.01.043.
19. Nguyen T. N. L., Le T. T., Ngo. T. D., Le. T. T. T., Ha. M. N., Nguyen. D. V., Bui M. Q., Nguyen. T. H. H., Nguyen. H. D., Nguyen. T. T., Le. T. L. - The size-and shape-controlled synthesis of silver nanoparticles by solvothermal method, Vietnam J. Sci. Technol **61** (2) (2023) 246-254. https://doi.org/10.15625/2525-2518/16615.
20. Poudyal N., Chaubey., Nandwana., Rong C., Yano K., Liu J. P. - Synthesis of FePt nanorods and nanowires by a facile method, Nanotechnology **19** (35) (2008) 355601. https://doi.org/10.1088/0957-4484/19/35/355601.
21. Yin Y., Alivisatos A. P. - Colloidal nanocrystal synthesis and the organic-inorganic interface, Nature **437** (2005) 664-670. https://doi.org/10.1038/nature04165.
22. Polavarapu L., Liz-Marzan L. M. - Growth and galvanic replacement of silver nanocubes in organic media, Nanoscale **5** (10) (2013) 4355-4361. https://doi.org/10.1039/C3NR01244A.
23. Li. H. J., Hui-Jun L., An-Qi Z., Yang H., Li S., Dong-Jin Q., Meng C. - Large-scale synthesis and self-organization of silver nanoparticles with Tween 80 as a reductant and stabilizer, Nanoscale Res. Lett. **6;7** (1) (2012) 1-13. https://doi.org/10.1186/1556-276x-7-612.
24. Yamashita Y., Miyahara R., Sakamoto K. - Emulsion and emulsification technology. cosmetic science and technology: Theoretical principles and applications , Elsevier Inc., 2017, pp. 489-506.
25. Qingbo Z., Jim Y. L., Jun Y. - Size and composition tunable Ag-Au alloy nanoparticles by replacement reactions, Nanotechnol **18** (24) (2007) 245605-245612. https://doi.org/10.1088/0957-4484/18/24/245605.
26. Feldheim J. P. N. - Assembly of phenylacetylene-bridged silver and gold nanoparticle arrays, JACS **122** (16), (2000) 3979-3980. https://doi.org/10.1021/ja000477a.
27. Pham. T. T. H., Nguyen. D. D., Vu X. H. - Facile synthesis of silver/gold alloy nanoparticles for ultra-sensitive rhodamine B detection, RSC Adv. **11** (35) (2021) 21475-21488. https://doi.org/10.1039/D1RA02576G.
28. Nguyen. T. N. L., Ngo T. D., Le T. T. T., Le T. T., Nguyen P. H., Nguyen D. V., Ngo T. H., Pham. H. N., Le V. T., Nguyen V. D., Le G., N., Nguyen V. D., Nguyen X. P., Le D. T., Nguyen T. K. T., Le T. L. - Synthesis and properties of hollow Fe_3O_4@Au hybrid nano-structures for T1-T2 MR imaging and a combination of magnetic and photo-induced heating, New J. Chem. **47** (2023) 4052-4067. https://doi.org/10.1039/D2NJ04880A.